THE JOURNAL OF BIOLOGICAL CHEMISTRY VOL. 286, NO. 20, pp. 18013–18025, May 20, 2011

Crystal Structure of Leukocyte Ig-like Receptor LILRB4 (ILT3/LIR-5/CD85k)

*A MYELOID INHIBITORY RECEPTOR INVOLVED IN IMMUNE TOLERANCE**

Received for publication, January 12, 2011, and in revised form, March 15, 2011 Published, JBC Papers in Press, March 30, 2011, DOI 10.1074/jbc.M111.221028

Hao Cheng[‡§], Fiyaz Mohammed[¶], Gol Nam[‡§], Yong Chen[‡§], Jianxun Qi[‡‖], Lee I. Garner[¶], Rachel L. Allen[**], Jinghua Yan[‡], Benjamin E. Willcox[¶1], and George F. Gao[‡§‖2]

From the [‡]CAS Key Laboratory of Pathogenic Microbiology and Immunology, Institute of Microbiology, Chinese Academy of Sciences, Beijing 100101, China, [§]Graduate University, Chinese Academy of Sciences, Beijing 100149, China, [¶]Birmingham CRUK Cancer Centre, School of Cancer Sciences, University of Birmingham, Vincent Dr., Edgbaston, Birmingham, B15 2TT, United Kingdom, the [**]Centre for Infection, Division of Cellular and Molecular Medicine, St. Georges, University of London, London, United Kingdom, and the [‖]Research Network of Immunity and Health, Beijing Institutes of Life Science, Chinese Academy of Sciences, Beijing 100101, China

The myeloid inhibitory receptor LILRB4 (also called ILT3, LIR-5, CD85k), a member of the leukocyte immunoglobulin-like receptors (LILRs/LIRs), is an important mediator of immune tolerance. Up-regulated on tolerogenic dendritic cells, it has been shown to modulate immune responses via induction of T cell anergy and differentiation of $CD8^+$ T suppressor cells and may play a role in establishing immune tolerance in cancer. Consequently, characterizing the molecular mechanisms involved in LILRB4 function and in particular its structure and ligands is a key aim but has remained elusive to date. Here we describe the production, crystallization, and structure of the LILRB4 ectodomain to 1.7 Å using an expression strategy involving engineering of an additional disulfide bond in the D2 domain to enhance protein stability. LILRB4 comprises two immunoglobulin domains similar in structure to other LILRs; however, the D2 domain, which is most closely related to the D4 domains of other family members, contains 3_{10} helices not previously observed. At the D1-D2 interface, reduced interdomain contacts resulted in an obtuse interdomain angle of ~107°. Comparison with MHC class I binding Group 1 LILRs suggests LILRB4 is both conformationally and electrostatically unsuited to MHC ligation, consistent with LILRB4 status as a Group 2 LILR likely to bind novel non-MHC class I ligands. Finally, examination of the LILRB4 surface highlighted distinctive surface patches on the D1 domain and D1D2 hinge region, which may be involved in ligand binding. These findings will facilitate our attempts to precisely define the role of LILRB4 in the regulation of immune tolerance.

The balance between activation and inhibition of effector immune responses is pivotal for appropriate regulation of the immune system and is crucial for maintaining the health of the host. Although initiation of the immune response by innate immune receptors has been relatively well studied (1), the factors underlying induction of immune tolerance are relatively poorly understood but are highly relevant to understanding immune responses during infection, malignancy, and autoimmune disease (2, 3). In addition to central tolerance, whereby thymocytes with high affinity for self-peptide/major histocompatibilty complex (MHC) complexes are deleted during T cell development in the thymus (4), complex tolerance mechanisms exist to control immune responses in the periphery. In particular, regulatory T lymphocyte cells (Treg) and tolerogenic antigen-presenting cells are central in this regard (5, 6). As well as $CD4^+CD25^+FoxP3^+$ Tregs, a distinct population of $CD8^+$ T cells with suppressive activity, characterized by their lack of CD28, has also been identified and termed T suppressor cells (7, 8). How critical tolerogenic signals are transmitted from regulatory populations to effector cells is not completely understood, although it is clear that both soluble mediators of tolerance, for example interleukin-10 and transforming growth factor-β, as well as cell-cell contact mechanisms utilizing regulatory immune receptors and their ligands, are involved. A comprehensive understanding of these issues is crucial and may enable rational design of therapeutic strategies that suppress tolerance mechanisms during malignancy or pathogen infection and stimulate tolerance mechanisms during autoimmunity or after transplantation.

The leukocyte immunoglobulin-like receptors (LILRs/LIRs),[3] also called immunoglobulin-like transcripts (ILTs) (9–12) or CD85 (13), are a family of regulatory immune receptors expressed predominantly on myeloid subsets, with emerging roles in the regulation of immune tolerance, in addition to their other known functions (14). Encoded in the leukocyte receptor cluster on human chromosome 19 (15), they are structurally and functionally related to other leukocyte receptor cluster receptors, such as the killer cell immunoglobulin-like

* This work is supported by grants from Ministry of Science and Technology of China (MOST, 973 Project 2010CB911902) and National Natural Science Foundation of China Grant 31030030.

The atomic coordinates and structure factors (code 3P2T) have been deposited in the Protein Data Bank, Research Collaboratory for Structural Bioinformatics, Rutgers University, New Brunswick, NJ (http://www.rcsb.org/).

[1] The laboratory work of B. E. W. is supported by Biotechnology and Biological Sciences Research Council project grant funding (Grant BB/E009417/1).

[2] A leading principal investigator of the National Natural Science Foundation of China Innovative Research Group (Grant 81021003). To whom correspondence should be addressed: CAS Key Laboratory of Pathogenic Microbiology and Immunology, Institute of Microbiology, Chinese Academy of Sciences, Beijing 100101, China. Tel.: 86-10-64807688; Fax: 86-10-64807882; E-mail: gaof@im.ac.cn.

[3] The abbreviations used are: LIR/LILR, leukocyte immunoglobulin-like receptors; ILT, immunoglobulin-like transcripts; HLA, human leukocyte antigen.

receptors, and have been reported to regulate a broad range of cells involved in the immune response (13, 16–20). In addition, the LILR family is relatively conserved evolutionarily, consistent with important immune functions (15, 21, 22). The LILR family has 13 members (including two pseudo-genes), characterized by different transmembrane and cytoplasmic domains, delivering either activating or inhibitory signals (11, 12, 16). Inhibitory LILR members have a long cytoplasmic tail containing different sets of immunoreceptor tyrosine-based inhibitory motifs that recruit phosphatases and thus contribute to downstream inhibitory signaling pathways (23, 24), whereas activating members have truncated cytoplasmic regions and are thought to associate with activating adaptor proteins via a positively charged amino acid in the transmembrane domain (*e.g.* LILRA2 and LILRA4 both associate with the γ chain of FcϵRI (25, 26)). The ligands for some of the LILRs are known, and the structural and biophysical basis of these recognition events have recently been resolved (27–33). LILRB1 (ILT2/LIR-1/CD85j) and LILRB2 (ILT4/LIR-2/CD85d) interact with both classical and non-classical MHC class I molecules and the class I-like molecule UL18 encoded by the human cytomegalovirus (30, 32, 33). Based on the analysis of the structure of LILRB1 (ILT2/LIR-1/CD85j) in complex with human leukocyte antigen (HLA)-A2/β_2m, Willcox *et al.* (32) proposed the two-group classification of the family. So-called "Group 1" receptors, which include LILRB1 (ILT2/LIR-1/CD85j), LILRB2 (ILT4/LIR-2/CD85d), LILRA1 (LIR-6/CD85i), LILRA2 (ILT1/LIR-7/CD85h), and LILRA3 (ILT6/LIR-4/CD85e), were noted to have high conservation of MHC binding residues and were hypothesized to interact with MHC class I or MHC class I-like proteins. In contrast, "Group 2" family members, which include LILRB3 (ILT5/LIR-3/CD85a), LILRB4 (ILT3/LIR-5/CD85k), LILRB5 (LIR-8/CD85c), LILRA4 (ILT7/CD85g), LILRA5 (ILT11/LIR-9/CD85f), and LILRA6 (ILT8/CD85b), have low conservation of such residues and are thought to recognize novel ligands not associated with β_2-microglobulin (32). A recent study appears to have confirmed this prediction for the Group 2 receptor LILRA4 (ILT7), which was shown to negatively regulate Toll-like receptor-mediated plasmacytoid dendritic cell function by binding to bone marrow stromal cell antigen 2 (BST2) (34). This finding highlights the potential importance of Group 2 LILRs in regulation of myeloid/dendritic cell function and emphasizes the requirement for a more detailed molecular understanding of these poorly characterized receptors.

A substantial body of data has highlighted the Group 2 receptor LILRB4 (ILT3/LIR-5/CD85k) (35), which is expressed on dendritic cells, monocytes, and macrophages, as playing an important role in the regulation of immune tolerance (36–39). In particular, T suppressor cells were found to induce the upregulation of expression of LILRB4 and LILRB2 on antigen-presenting cells (35, 39–43), rendering them tolerogenic to T cells. In addition, recombinant LILRB4-Fc has also been shown to modulate T cell responses via induction of T helper cell (Th) anergy and differentiation of $CD8^+$ T suppressor cells (44), and soluble LILRB4 has been detected in the blood of patients with cancer and can promote tolerance of tumor grafts in a humanized mouse model (44, 45). However, the molecular basis of such effects is unclear, because in contrast to LILRB2, both the ligands and structure of LILRB4 have remained elusive. Interestingly, LILRB4 is somewhat unusual as whereas most family members contain four Ig-like domains in their extracellular region (designated D1, D2, D3, and D4), LILRB4 is one of two members that only possess two Ig-like domains (the other one is the closely related activating receptor LILRA5 (46)). In addition, previous studies found that LILRB4 behaves as an "outlier" in family phylogenetic analysis (15). Collectively, these findings strongly justify further investigation of the structure and function of this important regulatory receptor.

To shed light on the function of LILRB4, we carried out recombinant expression of its complete extracellular domain and introduced a new disulfide bond to stabilize the protein for crystallization, a strategy we previously applied to LILRA2 (28). Using this approach, we successfully crystallized LILRB4 and here report its crystal structure to 1.7 Å. Our results show that the LILRB4 ectodomain adopts an unusually obtuse interdomain angle, which is stabilized by poor hydrophobic interactions, relative to other LILRs. They also reveal novel 3_{10} helical regions in the D2 domain, which is most closely related in sequence to the D4 domain of other LILRs. Finally, our analyses indicate that LILRB4 has a tertiary structure and surface charge distribution unsuitable for binding MHC class I proteins and highlight two distinct surface patches, on the D1 domain and at the D1D2 hinge region, that may form components of a ligand binding site.

EXPERIMENTAL PROCEDURES

Cloning and Stability Engineering of LILRB4—DNA encoding the extracellular region of LILRB4 (residues 1–196 of the mature protein, comprising the two Ig-like domains, termed D1 and D2) was amplified by PCR using the forward primer LILRB4Fw (5′-CCAACATATGGGGCCCCTCCCCAAACCC-3′) and the reverse primer LILRB4Rv (5′- CCGCTCGAGTTAT-CCTGAGACTATGAGCTCCAGGGGGTC-3′), which introduced non-coding mutations to limit RNA secondary structure and improve codon usage as previously described (47). PCR products were digested with NdeI and XhoI and ligated into the pET21a plasmid vector (Novagen). DNA fragments corresponding to stability-engineered LILRB4 D1D2 mutant (I133C, H143C, termed the LILRB4cc mutant, see "Results" section) were generated by PCR mutagenesis using the LILRB4 D1D2-pET21a plasmids as templates and the following primers (mutated nucleic acids are shown in bold and underlined): LILRB4mu1, CTTCTG**TG**CAAGGAGCGGGCAGCCCATC-CCCTACTG**TG**TCTGAGATC; LILRB4mu2, GATCTCAGA-**CA**CAGTAGGGGATGGGCTGCCCGCTCCTTG**CA**CAG-AAG. PCR products corresponding to LILRB4cc were digested and ligated into pET21a as described above.

Expression and Purification of both LILRB4wt and LILRB4cc—Inclusion bodies of both recombinant proteins were expressed in *Escherichia coli* strain BL21(DE3) pLysS and prepared using existing protocols (47–49). Briefly, the inclusion bodies were washed with washing buffer (0.5% Triton X-100, 50 mM Tris-HCl, pH 8.0, 300 mM NaCl, 10 mM EDTA, 10 mM β-mercaptoethanol (β-ME), and 0.1% NaN_3), resuspension buffer (50 mM Tris, pH 8.0, 100 mM NaCl, 10 mM EDTA, 10 mM β-ME, and

0.1% NaN_3) and then dissolved overnight in a denaturing buffer (6 M guanidine hydrochloric, 50 mM Tris-HCl, pH 8.0, 100 mM NaCl, 10 mM EDTA, 10% (v/v) glycerin, and 10 mM DTT). The inclusion bodies were renatured by dilution refolding at 4 °C using the following refolding buffer: 100 mM Tris-HCl, 2 mM EDTA, 400 mM L-arginine-HCl, 0.5 mM oxidized glutathione, 5 mM reduced glutathione, 0.1 mM PMSF, and 0.1 mM NaN_3, with the pH adjusted to 8.0. The refolding solution was incubated overnight and then concentrated using a stirred cell and ultracentrifugal filter devices (Millipore). Refolded protein was purified by size exclusion chromatography using a HiLoad™ Superdex 75 16/60 PG column with AKTA FPLC (GE Healthcare).

Analytical Ultracentrifugation Analysis—Analytical ultracentrifugation was performed on a Beckman XL-A analytical ultracentrifuge (Fullerton, CA). The protein samples (LILRB4wt and LILRB4cc) were used at an initial concentration of $A_{280} = 1.0$ absorbance units and dissolved in 20 mM Tris-Cl, 150 mM NaCl, pH 8.0. Samples (400 μl) and reference solutions (400 μl, 20 mM Tris-Cl, 150 mM NaCl, pH 8.0) were loaded into a conventional double-sector quartz cell and mounted in a Beckman Coulter An-60 Ti 4-hole rotor. Sedimentation velocity experiments were performed at a speed of 54,000 rpm. The protein profiles were measured by UV absorbance at 280 nm in a continuous mode with time intervals of 480 s. The recorded scans for the various time points were collected and analyzed using the c(s) continuous size distribution model with the SEDFIT program Version 11.3b (50). Molecular weights were estimated using the c(M) model after fitting the frictional ratio (f/f_0).

Multiple Alignments and Phylogenetic Analysis—To investigate the evolutionary relationships of the LILR family, we analyzed sequences of the 13 family members (including the two pseudo-genes, LILRP1 (ILT 9) and LILRP2 (ILT10)) using the following accession codes of protein in GenBank™: LILRA2, Q8N149; LILRB1, Q8NHL6; LILRB4, Q8NHJ6; LILRB2, Q8N423; LILRB3, O75022; LILRA3, Q8N6C8; LILRA4, P59901; LILRA6, Q6PI73; LILRP1, AF072102; LILRP2, AAC99762; LILRA5, A6NI73; LILRA1, O75019; LILRB5, O75023. We used LILRB1, LILRB2, and LILRA5 as reference templates to identify the different domains for each protein. Approximately, we defined the domains as follows: amino acids 23–118, domain 1 (D1); 119–219, domain 2 (D2); 220–318, domain 3 (D3); 319–420, domain 4 (D4). Multiple alignments were performed using ClustalX (Version 2.09) with the full protein sequence and D1D2, D3D4 and D4 fragments. Phylogenetic trees were prepared by Phylip (Version 3.67).

Crystallization and Data Collection—Both purified LILRB4wt and LILRB4cc were concentrated to 20 mg/ml in a buffer consisting of 20 mM Tris, pH 8.0, 50 mM NaCl. Initial screening of crystallization conditions was performed using sparse matrix approaches with commercial screening kits supplied by Hampton Research. All crystallization experiments were performed using the vapor diffusion method at both 18 and 4 °C.

Diamond-shaped crystals of LILRB4cc were obtained in hanging drops equilibrated against a reservoir solution containing 0.2 M sodium sulfate heptahydrate, 20% (w/v) polyethylene glycol 3350 at 4 °C. For data collection, ideal crystals were soaked in reservoir buffer supplemented with 15% (v/v) glycerol for 60 s before they were flash-cooled to 100 K in a nitrogen gas stream. X-ray diffraction data were collected to 1.7 Å resolution using an in-house Rigaku MicroMax007 x-ray generator (CuK_α; $\lambda = 1.5418$ Å) equipped with an R-AXIS IV++ image-plate detector. X-ray data were processed, scaled, and merged using the HKL2000 program package (51). Data processing statistics are listed in Table 1.

TABLE 1
Data processing and refinement statistics for LILRB4

	LILRB4
Data processing	
Space group	$P4_12_12$
Unit cell dimensions	$a = 61.86$, $b = 61.86$, $c = 115.83$ (Å) a = 90, $\beta = 90$, $\gamma = 90$ (°)
Resolution (Å)	50-1.7 (1.76-1.7)[a]
Observed reflections	172,331 (11,061)
Unique reflections	24,975 (2,458)
Multiplicity	6.9 (4.5)
Completeness[b] (%)	98.2 (98.6)
R_{merge}[c] (%)	5.0 (23.7)
$I/\sigma(I)$	33.8 (6.8)
Refinement	
Resolution (Å)	22.5-1.7
R_{factor}[d] (%)	18.7
R_{free}[e] (%)	21.8
Root mean square deviations	
Bond lengths (Å)	0.004
Bond angles (°)	0.943
B-factors (Å^2)	
Protein	23.5
Water	33.7

[a] Numbers in parentheses apply to data in the highest resolution shell.
[b] Completeness = (number of independent reflections)/(total theoretical number).
[c] $R_{merge}(I) = (\Sigma|I(i) - \langle I(h)\rangle|/\Sigma I(i))$, where $I(i)$ is the ith observation of the intensity of the hkl reflection, and $\langle I\rangle$ is the mean intensity from multiple measurements of the h, k, l reflection.
[d] $R_{factor}(F) = \Sigma_h||F_{obs}(h)| - |F_{calc}(h)||/\Sigma_h|F_{obs}(h)|$, where $|F_{obs}(h)|$ and $|F_{calc}(h)|$ are the observed and calculated structure factor amplitudes for the h, k, and l reflection.
[e] R_{free} is calculated over reflections in a test set not included in atomic refinement.

Structure Determination and Refinement—The crystal belonged to the tetragonal space group $P4_12_12$ (unit cell constants: $a = b = 61.86$ Å, $c = 115.83$ Å, $\alpha = \beta = \gamma = 90°$), with one LILRB4cc molecule per asymmetric unit corresponding to 51.2% solvent content (52). The LILRB4cc structure was solved by molecular replacement using MOLREP (53) and PHASER (54) as previously described (29, 55). The search probe consisted of the LILRA5 structure (PDB code 2D3V) (31) with regions that are incompatible to LILRB4 and all flexible loops omitted. Unambiguous rotation and translation function solutions for each domain were found independently using data to 3.5 Å resolution.

Initial restrained rigid-body refinement was carried out using REFMAC5 (56), interspersed with iterative manual rebuilding with the program COOT (57). Subsequent $2F_o - F_c$ and annealed omit electron density maps allowed for the placement of all LILRB4 residues. After further cycles of refinement, the R_{factor} and R_{free} converged to 18.7 and 21.8%, respectively, for all data between 22.5 and 1.7 Å. The refinement statistics are listed in Table 1.

Ramachandran plot and secondary structure assignments were generated with SFCHECK (58). Analysis of the Ramachandran plot reveals that the LILRB4 model contains 90.1% of the residues in the most favored region, 9.3% in the additional

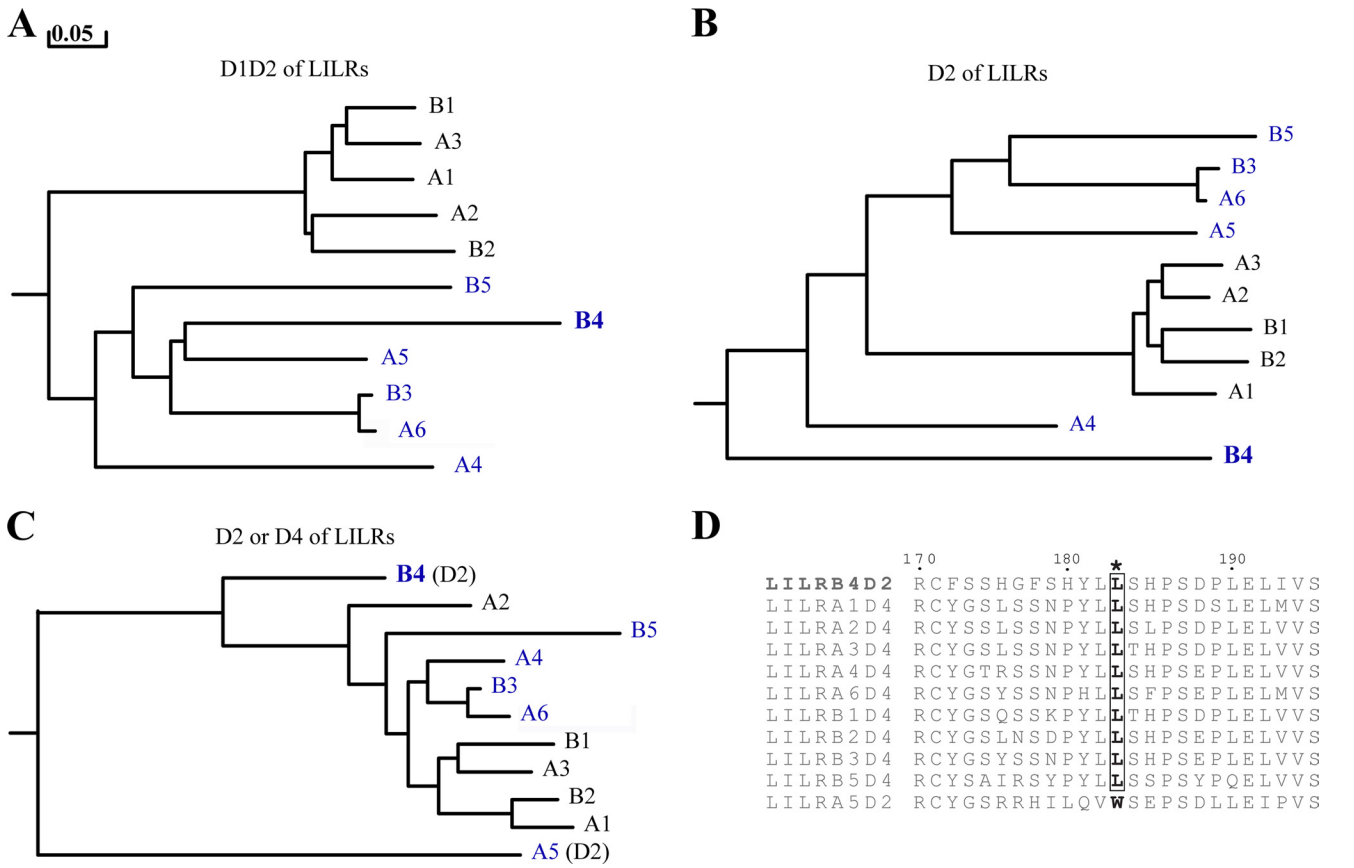

FIGURE 1. **Bioinformatic analysis of LILRB4.** Phylogenetic trees were generated using PHYLIP employing maximum likelihood methods. Analyses were based on comparison of D1D2, D2, and D4 sequences of LILR family members, omitting the two pseudo-genes LILRP1 (ILT9) and LILRP2 (ILT10). Group 1 members are labeled in *black*, and Group 2 members are shown in *blue*. A distance scale is included, in centimorgans. LILRB4 is shown in *bold* (*B4*). *A*, analysis of the D1-D2 domains of the LILR family highlights separate clusters of Group 1 and Group 2 receptors. *B*, shown is a comparison of D2 domains, indicating LILRB4 D2 represents an outlier. *C*, shown is a comparison of the D2 domain of LILRB4 and LILRA5 with the D4 domains of other LILRs, indicating LILRA5 D2 but not LILRB4 D2 is an outlier relative to the D4 domains of other family members. *D*, shown is alignment of the D2 domain of LILRB4 (*top*) and LILRA5 (*bottom*) with the D4 domains of other LILR receptors. The Leu/Trp residue is highlighted in *bold*, and residue numbering is for LILRB4.

allowed region, 0.6% in the generously allowed region, and no residues in the disallowed region. For analysis of interdomain angle and buried surface areas, D1 was defined as residues 1–96, and D2 was defined as residues 97–196, as for LILRA5 (31). Interdomain contact residues were identified using the program CONTACT (55) and were defined as residues containing an atom of ≤4.0 Å of the target partner. Buried surface areas were calculated using SURFACE (55) with a 1.4 Å probe radius. Figure were prepared with POVSCRIPT (59) and POV-RAY. Electrostatic surfaces were calculated using GRASP (60).

RESULTS AND DISCUSSION

Bioinformatic Analysis of the LILRB4 Ectodomain—To shed light on the distinct structural features of LILRB4, we compared the sequence of the LILRB4 ectodomain with that of other LILR receptors. Phylogenetic trees constructed on the basis of comparison of D1D2 fragment sequences highlighted a delineation between Group 1 receptors and Group 2 receptors, consistent with previous structural results that initially proposed the Group1/2 classification based on conservation (Group 1) or lack of conservation (Group 2) of amino acids involved in MHC class I binding (32). Consistent with its poor conservation of residues involved in MHC class I binding, comparison of the complete LILRB4 ectodomain sequence placed it close to other Group 2 receptors (Fig. 1*A*). More detailed analysis of the individual domains of the receptor highlighted that although the D1 domain bore similarity to other LILR D1 domains, the LILRB4 D2 domain shared highest identity with the D4 domains of other family members, as previously noted (9) (Fig. 1, *B* and *C*). In contrast, the D2 domain of LILRA5, the other Group 2 receptor with only 2 extracellular immunoglobulin domains, shared highest sequence identity with other LILR D2 domains (Fig. 1, *B* and *C*). In addition, alignment of the D2 domain of LILRB4 and LILRA5 with the D4 domains of other LILR receptors revealed LILRB4 shares a characteristic Leu residue with D4 domains, whereas LILRA5 has a Trp at this position, typical of all other LILR D2 domains (Fig. 1*D*). Because this Trp residue is important in mediating interdomain interactions in LILRs analyzed structurally to date, this suggested that LILRB4 may have an altered D1-D2 interdomain interface relative to other LILRs. Therefore, in summary, LILRB4 is distinguished by an unusual domain organization comprising a classical LILR D1 domain juxtaposed to an immunoglobulin domain that is most similar to the membrane-proximal D4 domain of other LILR receptors.

Stability Engineering Facilitates the Crystallization of LILRB4—Previously, the extracellular domain of wild type LILRB4 D1D2

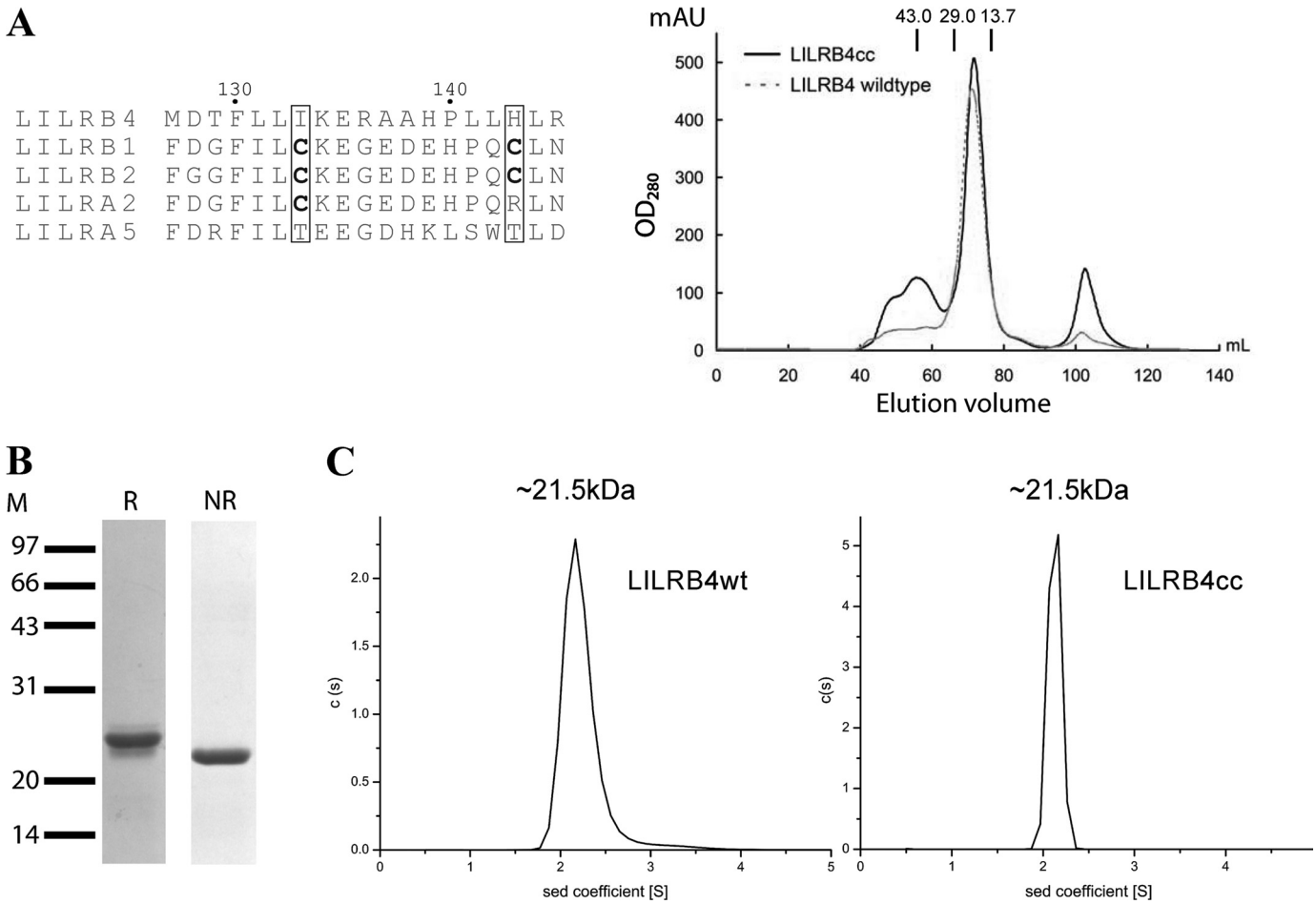

FIGURE 2. **Biochemical and biophysical characterization of LILRB4wt and LILRB4cc proteins.** *A*, mutated sites and introduced disulfide bond are indicated (*left panel*) with size exclusion chromatography elution profiles of refolded LILRB4wt and LILRB4cc proteins (*right panel*). The LILRB4wt and LILRB4cc size exclusion chromatography profiles are shown in *solid* and *dashed lines*, respectively. The profiles are marked along with approximate positions of molecular mass standards of 43.0, 29.0, and 13.7 kDa. *B*, reducing (*R*) and non-reducing (*NR*) SDS-PAGE analysis of refolded size exclusion-purified LILRB4 proteins. *C*, sedimentation velocity analytical ultracentrifugation profiles of LILRB4wt (*left*) and LILRB4cc (*right*) show the sedimentation coefficient distribution analysis c(s) and the corresponding molecular weights, as determined from size distribution (c(M)) analyses.

(LILRB4wt) was produced using *E. coli* expression and refolding approaches for structural and ligand identification analyses. Although pure, antibody-reactive material was produced to high levels (48) (Fig. 2), its stability was limited *in vitro*, and it showed pronounced precipitation during concentration steps. Despite great efforts, attempts at LILRB4 D1D2 crystallization only produced microcrystals (47), and diffraction quality crystals were not obtained. These results suggested alternative strategies might be required for successful LILRB4 D1D2 structural analysis.

Inspection of the LILRB4 sequence in relation to other LILRs indicated conservation of canonical cysteines in D1 (at 26 and 75) and D2 (at 121 and 172) that form intradomain disulfide bonds. However, LILRB1 and LILRB2, which both crystallized readily, contained an additional pair of Cys residues in the C-C′ loop in D2 that formed a second intrachain disulfide in the D2 domain. In contrast, LILRB4 lacked these additional cysteines, the corresponding C-C′ loop residues being Ile-133 and His-143 (Fig. 2*A*). In previous work on LILRA2, we overcame the obstacle of LILRA2 instability by introducing a Cys residue to form an additional disulfide bond in this D2 C-C′ loop, which enhanced the production of the D1D2 of LILRA2, allowing crystallization and structure solution (28). This disulfide bond was found to make the neighboring loop region less flexible without influencing the overall topology of the structure (61). We hypothesized that, as for LILRA2, the absence of such a bond may result in high flexibility of this region, decreasing protein stability and inhibiting crystallization. To rectify this, we introduced an artificial disulfide bond in this region by using site-directed mutagenesis to generate the mutations I133C and H143C, resulting in a protein termed LILRB4cc. The engineered LILRB4cc protein was found to have higher stability, could be concentrated to much higher levels than the wild type (LILRB4wt), and displayed much less precipitation during concentration steps. To exclude the possibility that the Cys residues introduced by the site-directed mutations caused the recombinant production of LILRB4 to behave abnormally, we compared the profile of the LILRB4wt and LILRB4cc proteins on size exclusion chromatography (Fig. 2, *A* and *B*) and analytical ultracentrifugation (Fig. 2*C*). LILRB4wt and LILRB4cc proteins eluted at essentially identical volumes on size exclusion (Fig. 2*A*), consistent with a similar overall size and shape. In addition, the peaks eluted between the 29.0- and 13.7-kDa marker proteins, indicating that both LILRB4wt and LILRB4cc

(MW ~21 kDa) behave as monomers in solution. Also, sedimentation velocity analytical ultracentrifugation measurements of both LILRB4wt and LILRB4cc proteins (Fig. 2*C*) indicated for each sample a single predominant species in the sedimentation coefficient distribution c(S), and transformation to a molar mass distribution c(M) confirmed a similar peak mass ~21 kDa, confirming each protein was monomeric in solution. Furthermore, the more convergent profile of the LILRB4cc (Fig. 2*C*, *right panel*) protein also suggested that relative to LILRB4wt (Fig. 2*C*, *left panel*), LILRB4cc had more restricted flexibility.

Extensive crystallization trials of native LILRB4 D1D2 suggested the protein was intransigent to crystallization. Moreover, this protein was clearly susceptible to proteolytic cleavage between the D1 and D2 domains, as crystals of a fragment corresponding to the D1 domain resulted from trials of intact LILRB4 D1D2 protein, suggestive of substantial interdomain flexibility. Consistent with the higher stability and lower conformational flexibility of the LILRB4cc in solution, LILRB4cc crystallized readily at 4 °C, in contrast to wild type protein, allowing the LILRB4cc structure to be solved to 1.7 Å.

Overall Structure of LILRB4—The refined crystal structure of LILRB4 contained one molecule per crystallographic asymmetric unit. LILRB4 comprised two immunoglobulin-like domains, D1 and D2 (defined as residues 2–96, and 97–195), each composed of β strands arranged into two anti-parallel β sheets, with one β-sheet containing three anti-parallel β-strands (A, B, and E) and the second containing five anti-parallel β-strands (C′, C, F, G, and A′). As expected, disulfide bonds were observed between Cys residues 26 and 75 in D1 and in D2 first between 121 and 172 as well as the additional artificial disulfide between position 133 and 143, analogous to the additional native disulfide observed in LILRB1/2 D2. Arguably the most striking feature of the structure was the interdomain angle. In contrast to the previous LILR structures, where the D1-D2 interdomain angles are ~84–90° in their ligand-free forms, the LILRB4 structure displayed an obtuse D1-D2 interdomain angle of 107° (Fig. 3, *A* and *B*). Comparison of the D1-D2 interdomain angles of LILRA5 (Fig. 3*B*, *left*), LILRB2 (Fig. 3*B*, *right*), and LILRB1, indicates the presence/absence of the additional disulfide between C and C′ in the LILR D2 domain does not correlate with the D1-D2 interdomain angle. Both LILRB1/B2 possess this disulfide in native form, whereas it is absent in LILRA5; notably all three receptors have an interdomain angle of ~90°. Therefore, the obtuse D1D2 interdomain angle observed in LILRB4 most likely reflects the distinct characteristics of the LILRB4 D1-D2 interface rather than being dependent on the non-native disulfide bond. Consistent with this, our studies on PD-L1 have shown that the angle between neighboring Ig domains can shift as a result of altered interactions of hydrophobic residues (62), as observed for LILRB4 compared with other family members (see below). These considerations strongly suggest that the unconventional orientation of LILRB4 D1-D2 domains reflects distinct intrinsic features of the interface of this two domain molecule.

The topology of the LILRB4 domains was similar to that of other LILRs but with some distinctive features (Fig. 3). In the D1 domain, LILRB4 displays some topological differences compared with LILRB1/2. In LILRB1/2, the region between the C and E strands, which in many immunoglobulin domains forms a strand termed D, instead includes helical secondary structural elements (29, 33). In contrast, in LILRB4 D1, the corresponding region is replaced by a β-strand termed C′ that pairs with strand C (Fig. 3*C*), as in the killer cell immunoglobulin-like receptors. Interestingly, recent studies have shown that the 3_{10} helix region between the C-E strands in LILRB2 D1 is directly involved in the recognition of the α3 domain of HLA-G (30), and the corresponding region of LILRB1 also forms interactions with the α3 domain of HLA-A2 (32). Alterations in this region of LILRB4 relative to LILRB1/2 could affect LILRB4 ligand interactions. Notably, the C′ strand we observe in LILRB4 has previously been noted in LILRA2 and LILRA5 (Fig. 3*D*), suggesting this topological feature can be present in both Group 1 and Group 2 receptors and in Group 2 is not restricted to LILRA5. In contrast to the loss of helical elements in this region in LILRB4, the 3_{10} helix observed between E and F strands in LILRB1/LILRB2/LILRA5 (29, 31, 33) is preserved in LILRB4.

In D2, LILRB4 displays two novel 3_{10} helical regions not previously observed in other LILR receptors; one located between the C-C′ strands and another between the E and F strands (Fig. 3*C*). For the C-C′ helix, we cannot exclude the possibility that introduction of the additional disulfide bond into this region affects that propensity for 3_{10} helix formation. However, notably LILRB1 and LILRB2 contain this additional disulfide in their native form and do not have a helix in this region, suggesting instead the divergent sequence of LILRB4 in this region relative to other LILRs may underlie this novel structural feature. Finally, in addition to 3_{10} helical regions, LILRB4 also contains a region of polyproline II helix in the F-G loop of each domain (Fig. 3*C*), and this is also present in LILRA2/5 and LILRB1/2 as well as other leukocyte receptor cluster receptors such as killer cell immunoglobulin-like receptors (63) and NKp46 (64).

Structural Features at the D1-D2 Interface—Previous studies have indicated the interdomain interface of LILR receptors is stabilized by both interdomain hydrogen bonds and hydrophobic interactions that are relatively conserved across the family (28, 29, 31, 33). For LILRB1, LILRB2, and LILRA5, the hydrophobic interdomain contact region comprises D1 residues from strands A′ (Val-15) and G (Val-94, Val-95 in LILRB1, equivalent to residues Val-93 and Met-94 of LILRB4) as well as residues from the 3_{10} helix located between the E and F strands (including Trp-67 and residues Ala-70, Gly-71, and Arg-72 in LILRB1), the G-A loop region that connects the D1 and D2 domains, and by D2 residues from the C′ strand (Leu-145 in LILRB1, equivalent to residue Leu-144 in LILRB4) and in the F strand (Tyr-175 in LILRB1, equivalent to residue Phe-173 in LILRB4) as well as the WS*X*PS motif (Leu-187, Pro-188 in LILRB1, equivalent to residues His-185 and Pro-186 of LILRB4). In addition to these amino acids, previous studies have highlighted two conserved D2 aromatic residues in the F-G loop, Tyr-183 and Trp-185 in LILRB1 (equivalent to residues Tyr-181 and Leu-183 in LILRB4, respectively), that contribute a majority of the interdomain interactions. Collectively, these interactions enable an interdomain interaction surface comparable in size to that of other leukocyte recep-

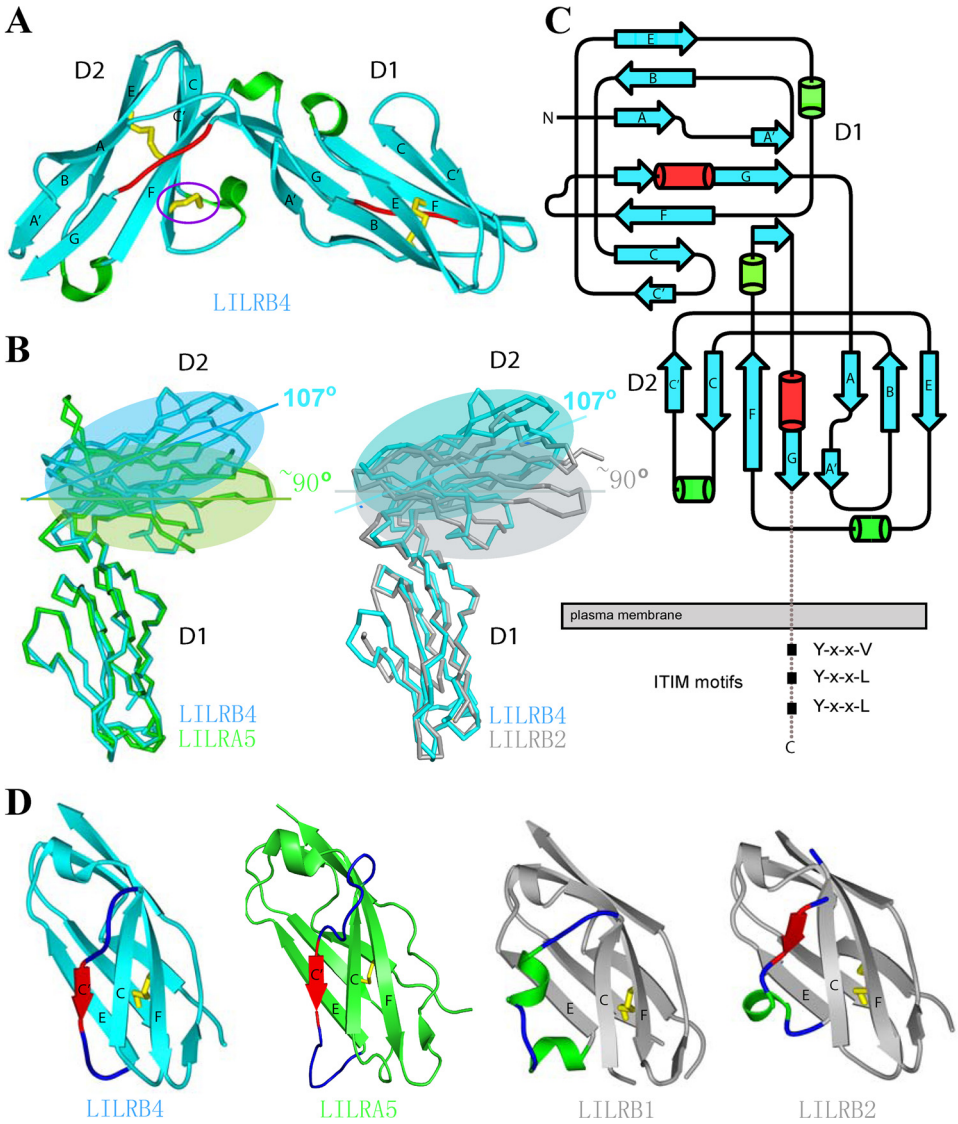

FIGURE 3. **Overall structure of the extracellular region of LILRB4.** *A*, shown is a ribbon diagram of the LILRB4 structure, with 3_{10} helices indicated in *green*, polyproline type II helices shown in *red*, disulfide bonds shown in *yellow*, and the introduced disulfide bond indicated by a *violet circle*. *B*, shown is a comparison of D1-D2 interdomain angle of LILRB4 with LILRA5 (*left panel*) and LILRB2 (*right panel*). LILRB4, LILRA5, and LILRB2 chains are shown in *cyan*, *green*, and *gray*, respectively. *C*, shown is a topological diagram of LILRB4 with 3_{10} helices indicated in *green* and polyproline type II helices indicated in *red*; the approximate orientation of the receptor relative to transmembrane and intracellular regions is shown. *D*, shown is a comparison of secondary structural elements in the D1 C-C′ region of LILRB4 (*cyan*), LILRA5 (*green*), LILRB1 and LILRB2 (*both gray*). Helical elements in the C-C′ region (only present in LILRB1 and LILRB2) are shown in *green*, and β strands are shown in *red*.

tor cluster-encoded receptors, with the total solvent-accessible area buried at the D1-D2 interface 946 Å^2 for LILRB1 (33) compared with 949 and 891 Å^2 for KIR2DL2 and NKp46, respectively (64, 65).

Analysis of the LILRB4 D1-D2 interdomain interface indicated a buried surface area of 866 Å^2 intermediate between that of LILRB1 (946 Å^2) and LILRB2 (776 Å^2) and comparable with LILRA5 (843 Å^2). Consistent with a broadly similar interdomain interface, the hydrogen bonding interactions present at the D1-D2 interface in LILRB1, LILRB2, and LILRA5 (from the D1 G strand to the short strand bearing Tyr-183 and Trp-185 (equivalent to Tyr-181 and Leu-183 in LILRB4, respectively)) were conserved in LILRB4. In addition, some important hydrophobic interactions are conserved, in particular contacts between Tyr-181 and residues Ala-70 and Arg-72 on or around the F strand (Fig. 4, *A* and *B*). However, several other hydrophobic interactions were altered. First, Trp-67, which in LILRB1 and LILRB2 mediates numerous hydrophobic interactions with Glu-184 for LILRB1 and Val-183 for LILRB2 (equivalent to LILRB4 Leu-182), is replaced in LILRB4 by Glu-67 (Fig. 4*B*, *top panels*). This decreases interdomain interactions, as Glu-67 mediates far fewer contacts to Leu-182. In addition, although LILRA5 also has a Glu at position 67, this mediates compensatory interactions with Phe-97, whereas this is not the case in LILRB4, as Phe is replaced with the shorter Ala at this position. A second alteration is at residue 173, which in LILRB4 is a Phe, as opposed to a Tyr at the equivalent position in LILRB1, LILRB2, and LILRA5 (Fig. 4, *A* and *B*). Although both side chains interact with Thr-95 (or the equivalent), Phe-173 in LILRB4 makes substantially fewer contacts. Finally, arguably the most significant alteration at the LILRB4 D1-D2 interface is substitution of Trp at 185 (present in LILRB1 and at the equiv-

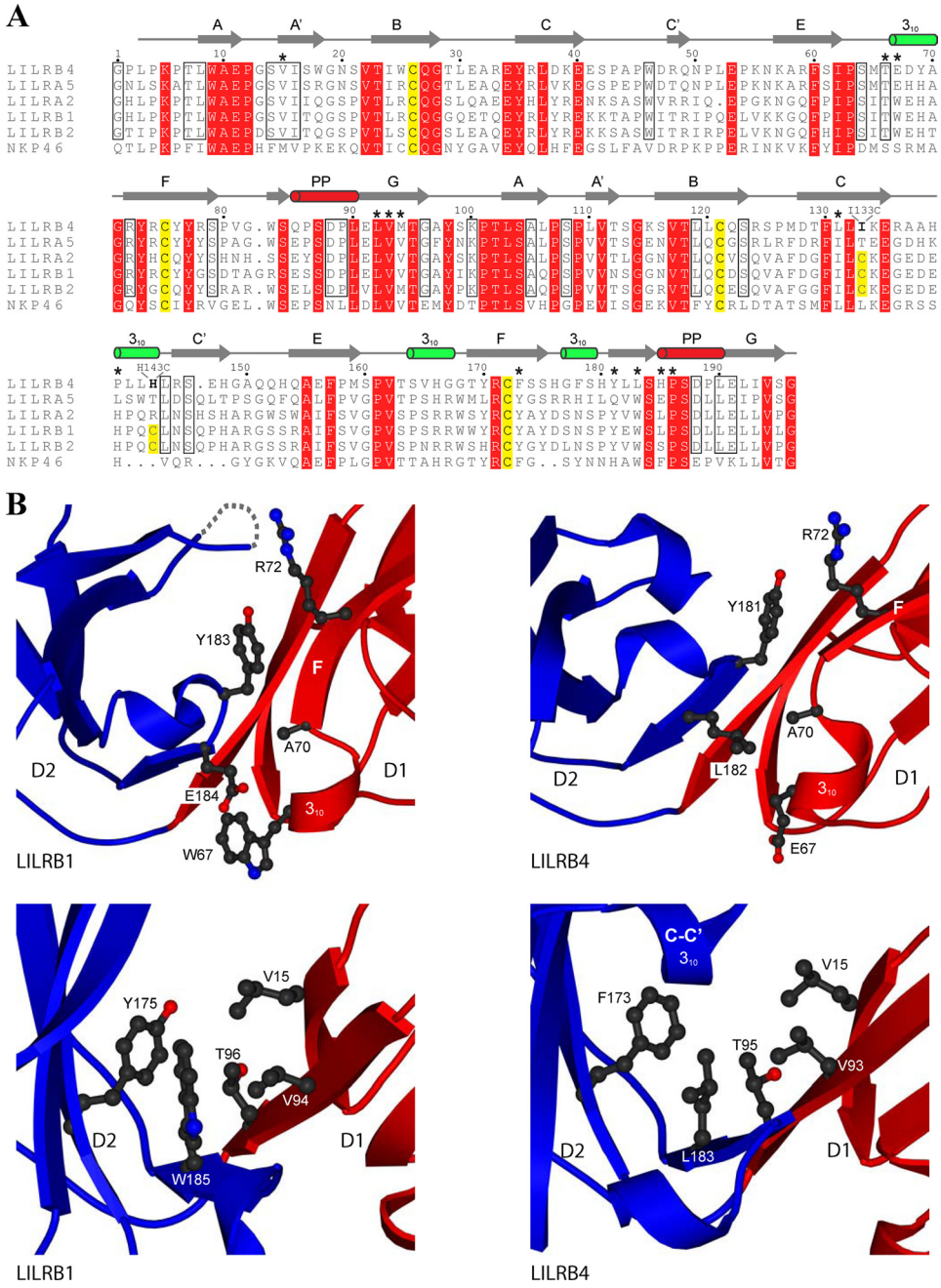

FIGURE 4. **Structural features at the LILRB4 D1D2 interface.** *A*, superimposition of LILRB4 and LILRB1/2, LILRA2/5, and NKp46, with LILRB4 residues involved in the D1D2 interdomain interface interactions marked with an *asterisk*. Residues conserved in all receptors are *shaded in red*. Cysteine residues involved in disulfide bonds are *shaded in yellow*, with the position of the engineered cysteines (I133C and H143C) indicated. Secondary structure elements of LILRB4 are shown *above the sequence*, with 3_{10} helices marked in *green* and polyproline type II helices (*PP*) depicted in *red*. The GenBank™ and PDB accession codes for each protein are, respectively: LILRB4 (Q8NHJ6, 3P2T); LILRA5 (A6NI73, 2D3V); LILRA2 (Q8N149, 2OTP); LILRB1 (Q8NHL6, 1G0X); LILRB2, (Q8N423, 2GW5); NKp46 (NP_004820, 1P6F). *B*, critical differences in the D1-D2 interfaces of LILRB1 and LILRB4 are shown. *Top left* and *top right* represent residues Trp-67, Ala-70, Arg-72, Tyr-183, and Glu-184 of LILRB1 and the equivalent residues of LILRB4, Glu-67, Ala-70, Arg-72, Tyr-181, and Leu-182, respectively. *Bottom left* and *bottom right* show residues Val-15, Val-94, Thr-96, Tyr-175, and Trp-185 from LILRB1 compared with Val-15, Val-93, Thr-95, Phe-173, and Leu-183 from LILRB4, respectively. For both receptors the D1 domain is shown in *red*, with D2 domain in *blue*. Amino acids involved in stabilizing the interdomain interface are highlighted in *ball and stick*.

alent 184 in LILRB2, LILRA5) to the less bulky Leu at the corresponding position 183 in LILRB4 (Fig. 4*B*, *lower panels*). Whereas Trp-185 forms extensive contacts to Val-15 and Val-94, the shorter size of the Leu-183 side chain in LILRB4 results in reduced contacts with these residues. To compare the different abilities of Leu and Trp to form packing interactions at the interdomain interface, we compared the number of contacts mediated by Leu and Trp in LILRB4 and LILRB1/LILRB2/LILRA5, respectively. Strikingly, Leu-183 of LILRB4 only makes 22 contacts to neighboring atoms (<4.00 Å), whereas the equivalent Trp-184 in LILRA5 forms 44 contacts. These observations indicate that the LILRB4 D1-D2 interface, although of a similar size to that of other LILR family members, involves considerably fewer stabilizing hydrophobic interac-

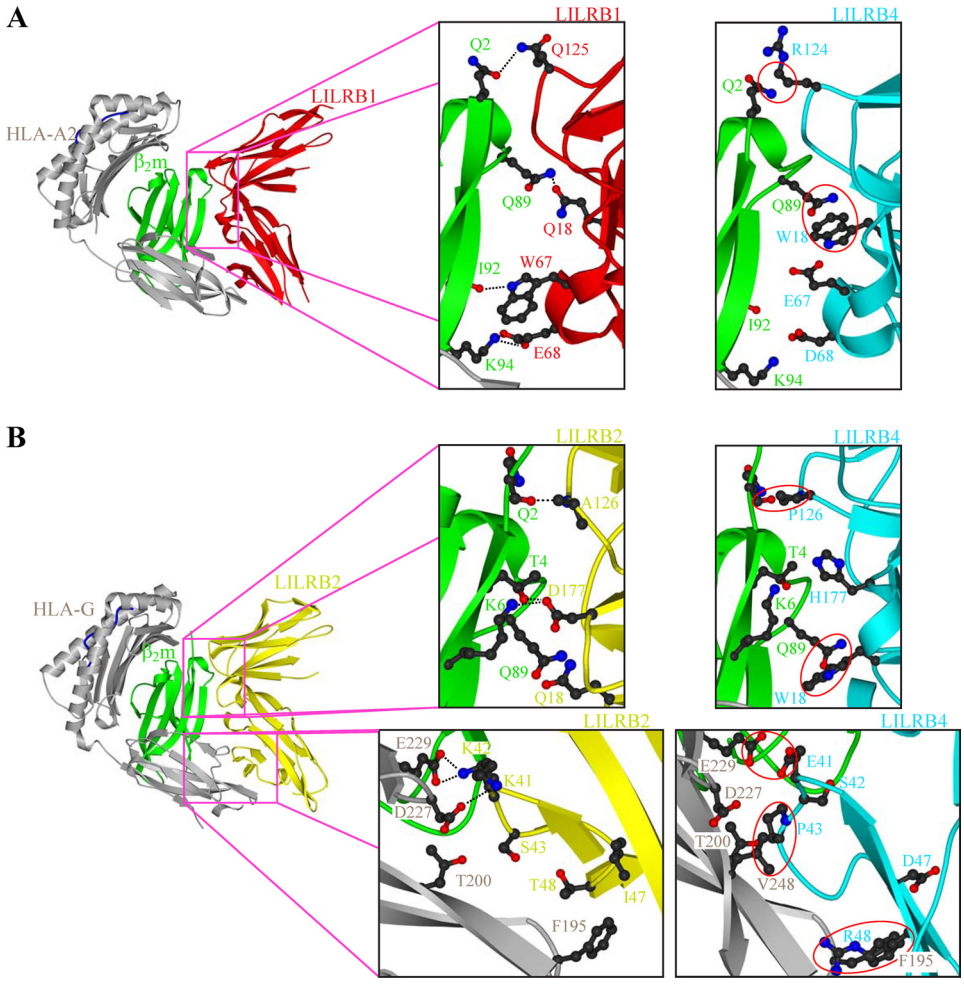

FIGURE 5. **Conformational incompatibility at the LILRB4/MHC class I interface.** *A*, shown is an analysis of the LILRB1/HLA-A2/β_2m interaction (*far left*) and expanded views of LILRB1 contacts with the β_2m moiety (*center*) and of critical changes at the hypothetical LILRB4/β_2m interface (*right*), with steric clashes indicated by *red circles*. The HLA-A2 heavy chain is shown in *gray*, and the β_2m moiety is shown in *green*, with LILRB1 in *red* and LILRB4 in *cyan*. *B*, analysis of the LILRB2/HLA-G/β_2m interaction (*far left*) is shown, with expanded views of LILRB2 contacts with the β_2m moiety (*top center*) and of critical changes at the LILRB4/β_2m interface (*top right*) The *lower expanded panels* show LILRB2 contacts at the HLA-G α3 domain (*center*) and relevant alterations at the hypothetical LILRB4/HLA-G/α3 interface (*right*). The HLA-G heavy chain is shown in *gray*, β_2m is in *green*, and LILRB2 and LILRB4 are in *yellow* and *cyan*, respectively. As in *A*, steric clashes are indicated by *red circles*.

tions. In addition, another distinct feature of the LILRB4 interdomain interface is involvement of residues from the unique LILRB4 D2 C-C′ 3_{10} helix (Fig. 4*B*, *lower right panel*) and in particular Pro-140, which is absent in other LILRs (see Fig. 3*C* and above). Because the novel 133–143 disulfide would be expected to stabilize this region of the molecule and the interdomain contacts it is involved in, this could explain why introduction of the novel disulfide favors crystallization, namely by reducing interdomain flexibility.

LILRB4 Is Conformationally and Electrostatically Unsuited for Recognition of MHC Class I—The crystal structures of LILRB1-HLA-A2 (32) and LILRB2-HLA-G complexes (30) showed that the ligand binding portion of LILRB1/2 comprises residues located in two distinct surface patches, first, a membrane distal portion of the D1 domain that forms contacts to the HLA α3 domain and, second, in the interdomain D1D2 hinge region, which contacts the β_2m domain. These interacting residues are highly conserved among Group 1 receptors but are extremely poorly conserved in Group 2 receptors including LILRB4 and LILRA5 (32). Determination of the LILRB4 structure allowed the conformation and electrostatic properties of these potential interaction surfaces to be examined as well as alterations in the LILRB4 interdomain orientation relative to MHC class I-bound forms of LILRB1 and LILRB2 to be assessed.

Superimposition of LILRB4 D1 and D2 onto the structure of LILRB1 in complex with HLA-A2 revealed a similar interdomain orientation; however, comparison of individual domain contacts to the HLA-A2 molecule provided a clear rationale for why this mode of MHC class I recognition would not be feasible for LILRB4. In terms of contacts with the α3 domain, in LILRB1, residues within strand C and the loop after strand C (including Tyr-38, Lys-41, and Thr-43) as well as Tyr-76 in the F strand form hydrophobic and van der Waals contacts to the α3 domain of HLA-A2 (residues Val-194, Ser-195, Asp-196, Thr-200, and Val-248). However, although in LILRB4 no drastic steric clashes are evident, not only are the relevant amino acids non-conservatively altered in many cases, but there are also secondary structural rearrangements, with a 3_{10} helix present in LILRB1 replaced by the C′ strand in LILRB4. Conse-

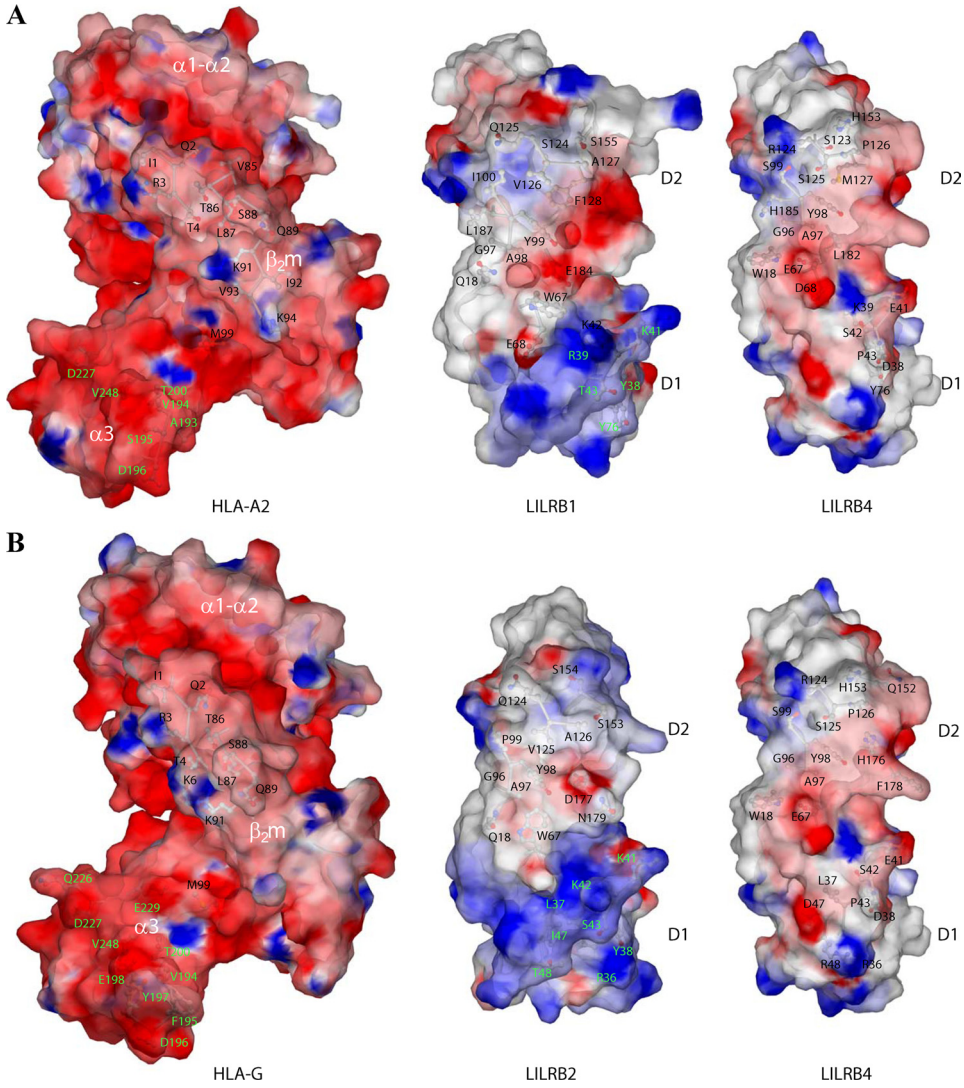

FIGURE 6. **Electrostatic incompatibility at the LILRB4/MHC class I interface.** *A*, shown are electrostatic surface representations of HLA-A2 (*left*), LILRB1 (*center*), and LILRB4 (*right*). *Red* is electronegative, and *blue* is electropositive. For HLA-A2/β_2m, amino acids involved in interaction with LILRB1 are indicated, with β_2m residues shown in *black* and α3 residues in *green*. LILRB1 residues involved in interaction with HLA-A2 are indicated, with those contacting β_2m residues in *black* and those contacting α3 residues shown in *green*. Equivalent residues on LILRB4 are all shown in *black*. *B*, shown are electrostatic surface representations of HLA-G/β_2m (*left*), LILRB2 (*middle*), and LILRB4 (*right*). As in *A*, HLA-G/β_2m amino acids involved in interaction with LILRB2 are indicated, with β_2m residues shown in *black*, α3 residues in *green*. LILRB2 residues involved in interaction with HLA-G are indicated, with those contacting β_2m residues in *black* and those contacting α3 residues shown in *green*. Equivalent residues on LILRB4 are all shown in *black*.

quently, the molecular contacts present at the LILRB1/α3 interface are likely to be lost for LILRB4.

At least as significant as these changes appears to be incompatibility at the LILR/β_2m interaction site, where amino acid changes in LILRB4 relative to LILRB1 would be predicted to result in steric clashes and loss of individual contacts (Fig. 5*A*). Whereas in LILRB1 Gln-18 hydrogen bonds to Gln-89 (β_2m), a non-conservative substitution to Trp-18 results in loss of this interaction and would cause a steric clash with Gln-89 (Fig. 5*A*). Similarly, whereas in LILRB1 the Gln-125 side chain hydrogen bonds with Gln-2 (β_2m), introduction of Arg-124 at the equivalent position in LILRB4 would abolish this interaction and sterically clash with Gln-2 (Fig. 5*A*). Also, whereas Trp-67 of LILRB1 hydrogen bonds with the backbone carbonyl of Ile-92 (β_2m), in LILRB4 a nonconservative substitution to the shorter Glu-67 would result in a loss of this contact as well as alter the electrostatic properties of the interaction surface (Fig. 5*A*). Finally, in LILRB4 there is an alteration to Asp at position 68, which in LILRB1 (Glu-68) forms a bidentate salt bridge with Lys-94 (β_2m). Although this change preserves the charge relative to LILRB1, introduction of the shorter Asp-68 side chain results in loss of these electrostatic interactions to Lys-94 (β_2m) (Fig. 5*A*).

A similar analysis reveals that the mode of HLA-G recognition adopted by LILRB2 is unfeasible for LILRB4 (Fig. 5*B*). Superposition of the LILRB4 D1 and D2 domains onto those of LILRB2 also highlighted a combination of steric clashes, loss of contacts, and electrostatic repulsion effects at the interaction surfaces, precluding a viable interaction. Relative to LILRB1 recognition of HLA-A2, LILRB2 forms more extensive contacts with the HLA-G α3 domain (in particular residues Tyr-197, Asp-227, Glu-229, and Thr-200) via residues in the loop after the C strand and the adjacent 3_{10} helix (Leu-37, Lys-41, Lys-42, and Ser-43). Superimposition of the D1 and D2 domains of

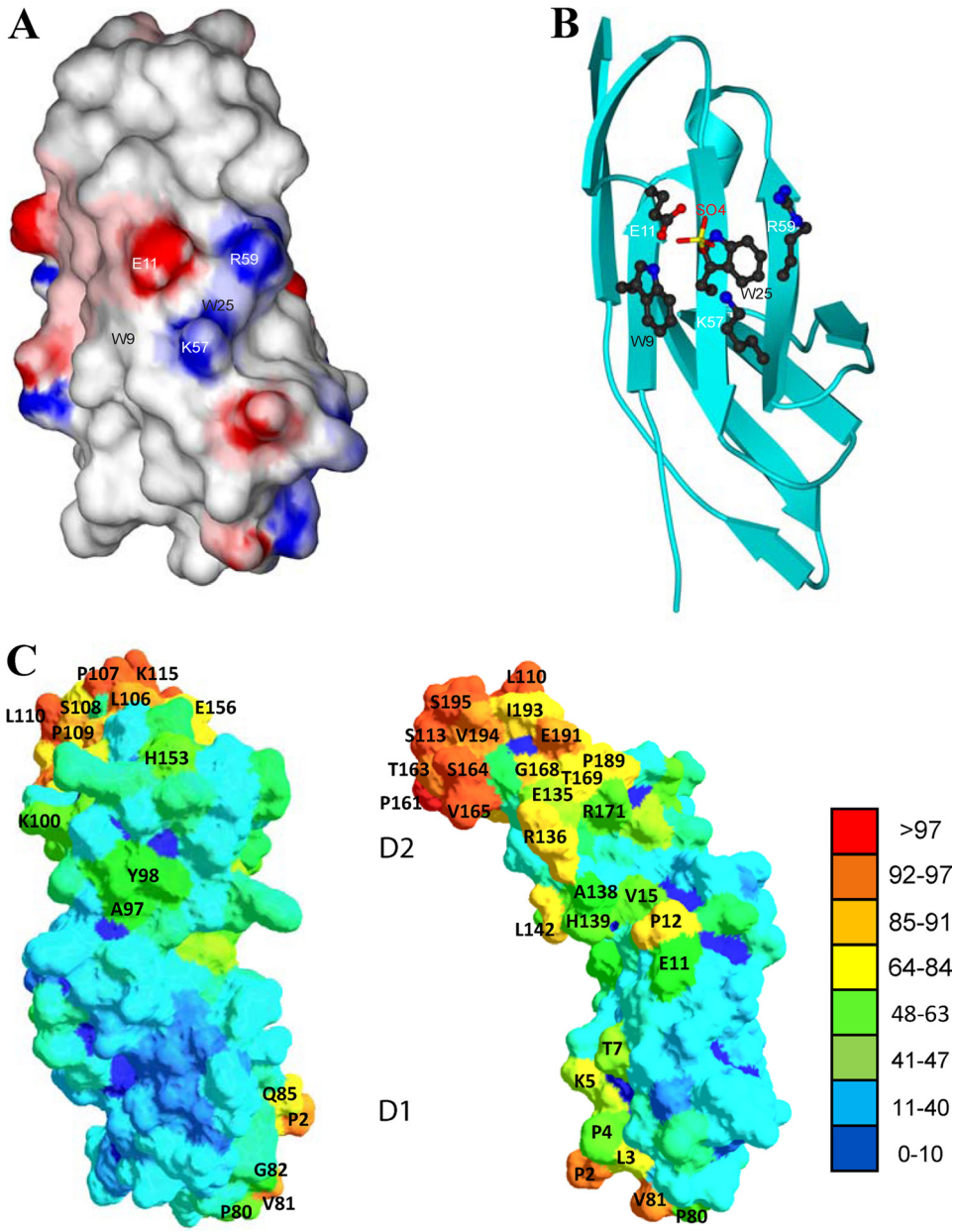

FIGURE 7. **Implications for LILRB4 ligand binding.** Analysis of LILRB4 residues that may be involved in ligand binding. *A*, shown is a potential ligand binding site on the ABE face (the solvent-exposed surface of A, B, and E β-strands) of the LILRB4 D1 domain, with surface tryptophans and adjacent charged residues indicated. *B*, shown is the interaction of the binding site in *A* with a sulfate ion in the LILRB4 crystal structure. *C*, SPPIDER analysis of the LILRB4 protein indicates three potential ligand interaction sites. The molecular surface is colored according to probability of interaction for each amino acid, as indicated in the key. Two views are shown: toward the CFG face of the D1 domain (*lower left panel*) or toward the ABE face (*lower right panel*). Residues of interest above the 50% probability are labeled.

LILRB4 onto those of LILRB2 bound to HLA-G reveals a number of steric clashes between LILRB4 residues comprising the C-C′ loop and C′ strand (Arg-36, Pro-43, Ala-44, Pro-45, and Arg-48) with HLA-G α3 residues (Fig. 5*B*, *lower panels*). In addition to these steric clashes, other substitutions lead to loss of further α3 contacts. Substitution of Lys-41 (LILRB2) to Glu-41 (LILRB4) eliminates a salt bridge to Asp-227 (HLA-G) and introduces likely electrostatic repulsion. Similarly, substitution of Lys-42 (LILRB2) to the smaller Ser-42 (LILRB4) eliminates a bidentate salt bridge to Glu-229 (HLA-G) with minimum chance of compensatory interactions. In addition, substitution of Ser-43 (LILRB2) to Pro-43 (LILRB4) causes a change in secondary structure that results both in steric clashes with Val-248 (HLA-G) and loss of contacts to Thr-200 (HLA-G). Finally, whereas Ile-47 and Thr-48 of LILRB2 stabilize the interface with HLA-G by mediating several hydrophobic contacts with Phe-195 (HLA-G), these are substituted to Asp-47 and Arg-48 in LILRB4, resulting both in loss of hydrophobic contacts (Arg-48 clashes with Phe-195) and radically different electrostatic properties for the interaction surface.

For the interaction surface with β_2m (Fig. 5*B*, *upper panels*), substitution of Ala-126 (LILRB2) to Pro-126 (LILRB4) eliminates hydrogen bonding with Gln-2 (β_2m) and introduces a potential steric clash. Also, substitution of Gln-18 (LILRB2) to

Trp-18 (LILRB4) results in a steric clash with Gln-89 (β_2m). Finally, substitution of Asp-177 (LILRB2) to His-176 (LILRB4) results in a loss of a salt bridge to Lys-6 (β_2m) and loss of a hydrogen bond to Thr-4 (β_2m).

Comparison of the electrostatic properties of the LILRB1 and LILRB2 surfaces that interact with HLA-A2 and HLA-G, respectively, indicated substantial differences with comparable regions of LILRB4, suggesting LILRB4 was unsuited for MHC class I recognition. Notably, the α3 region of the MHC class I heavy chain for both HLA-A2 and HLA-G contacted by the LILRs is predominantly negatively charged (Fig. 6, *A* and *B*) and features numerous acidic residues. The α3-interacting surface on both LILRB1 and LILRB2 is relatively positively charged (Fig. 6, *A* and *B*), and several interacting residues are basic, including Arg-39 and Lys-41 (on LILRB1) and Arg-36, Lys-41, and Lys-42 (on LILRB2), suggesting substantial electrostatic complementarity between the interacting surfaces. However, the comparable LILRB4 surface that would contact the α3 domain residues is considerably less positively charged than that of LILRB1 and LILRB2 (Fig. 6, *A* and *B*, *right panels*). Furthermore, within this surface, there is a Lys-41 → Glu-41 change that reverses charge and would introduce electrostatic repulsion at the interface with MHC class I. In addition, whereas in the LILRB2/HLA-G interaction hydrophobic interactions with the aromatic residue Phe-195 on HLA-G are mediated by Ile-47 and Thr-48 on LILRB2, in LILRB4 these are changed to Asp-47 and Arg-48, respectively, resulting in a highly charged surface in proximity to the hydrophobic HLA-G residue (Fig. 6*B*). Furthermore, Asp-177 on LILRB2 forms salt bridges to Lys-6 on HLA-G (β_2m), whereas in LILRB4 this residue is altered to His-176, eliminating this charged residue and the interactions it mediates. Therefore, the electrostatic properties of LILRB4 are unsuitable for recognition of MHC class I in comparison to the MHC class I-recognizing receptors LILRB1 and LILRB2.

These findings collectively suggest that the region of LILRB4 equivalent to the ligand binding surface of LILRB1 and LILRB2 is unsuited for MHC class I interaction both in terms of conformation and also the chemical nature of the surface. Consistent with these differences, neither LILRB4 nor the related Group 2 receptor LILRA5 shows significant binding to MHC class I molecules (31, 47).

Implications for Ligand Interactions Involving LILRB4—As well as illustrating the molecular diversity within the LILR family, the distinct structural features of LILRB4 relative to the MHC class I-recognizing receptors LILRB1 and LILRB2 may be important in allowing binding to novel non-MHC-like ligands. Although the ligands of LILRB4 are unknown, analysis of the LILRB4 structure highlighted two separate regions that could form components of an interaction surface or surfaces for ligand binding. First, manual inspection of the D1 domain highlighted a distinct group of residues on the ABE face (the solvent-exposed surface of A, B, and E β-strands) of the domain consisting of two surface-exposed hydrophobic residues (Trp-9 and Trp-25), with three charged groups in close proximity (Glu-11, Lys-57, and Arg-59) (Fig. 7*A*). In particular, the presence of two surface-exposed Trp residues seemed especially noteworthy. This site is relatively conserved across Group 2 LILRs (Trp-9, Glu-11, and Lys-57 are conserved; Trp-25 is conserved except in LILRA5, where it is altered to Arg; Arg-59 is largely conserved except in LILRB5 and LILRA4, where it is altered to Lys). Intriguingly, in the LILRB4 crystal structure this region was also found to interact with a sulfate anion (Fig. 7*B*). Although these features are suggestive of potential as an interaction surface, it is unclear how they relate to physiological ligand interaction.

Second, automated analysis of the LILRB4 ectodomain crystal structure was conducted using the SPPIDER (solvent accessibility based protein-protein interface Identification and recognition) algorithm, which can be used to predict residues at a putative protein interface by considering a single protein chain with a resolved three-dimensional structure. SPPIDER uses relative solvent accessibility-based methods and artificial neural networks for prediction of protein-protein binding sites based on discrepancies between predicted and observed (in an unbound protein structure) surface exposure of amino acid residues (66). SPPIDER analysis suggested 3 potential interaction surfaces (Fig. 7*C*) in LILRB4; 1 at the membrane-distal tip of the D1 domain (residues 2–5, 80–82, and 85), a second at the D1D2 hinge region (residues 11–15 and 138–142), and a third at the membrane proximal base of the D2 domain (principally 102–116, 158–165, and 189–195). Interestingly, the first and second sites are close to the D1 tip and D1D2 hinge region regions on LILRB1/LILRB2 involved in recognition of MHC class I proteins, respectively. This could suggest that the ligand binding surfaces of Group 2 receptors such as LILRB4 share features with Group 1 LILRs that recognize MHC class I. In contrast, its proximity to the membrane and the relatively short stalk region connecting the transmembrane domain to D2 in LILRB4 suggests site 3 may be principally involved in interactions with the plasma membrane rather than cognate ligand recognition. Finally, although SPPIDER predictions failed to match the surface highlighted by manual inspection, notably site 2 at the D1D2 hinge region also included Glu-11 and, therefore, overlapped minimally with this surface.

REFERENCES

1. Janeway, C. A., Jr., and Medzhitov, R. (2002) *Annu. Rev. Immunol.* **20,** 197–216
2. Prud'homme, G. J. (2004) *J. Leukoc. Biol.* **75,** 586–599
3. Kawai, T., and Akira, S. (2006) *Nat. Immunol.* **7,** 131–137
4. Nemazee, D. (2006) *Nat. Rev. Immunol.* **6,** 728–740
5. Belkaid, Y., and Oldenhove, G. (2008) *Immunity* **29,** 362–371
6. Sakaguchi, S., Yamaguchi, T., Nomura, T., and Ono, M. (2008) *Cell* **133,** 775–787
7. Filaci, G., Fravega, M., Negrini, S., Procopio, F., Fenoglio, D., Rizzi, M., Brenci, S., Contini, P., Olive, D., Ghio, M., Setti, M., Accolla, R. S., Puppo, F., and Indiveri, F. (2004) *Hum. Immunol.* **65,** 142–156
8. Liu, Z., Tugulea, S., Cortesini, R., and Suciu-Foca, N. (1998) *Int. Immunol.* **10,** 775–783
9. Borges, L., Hsu, M. L., Fanger, N., Kubin, M., and Cosman, D. (1997) *J. Immunol.* **159,** 5192–5196
10. Colonna, M., Navarro, F., Bellón, T., Llano, M., García, P., Samaridis, J., Angman, L., Cella, M., and López-Botet, M. (1997) *J. Exp. Med.* **186,** 1809–1818
11. Cosman, D., Fanger, N., Borges, L., Kubin, M., Chin, W., Peterson, L., and Hsu, M. L. (1997) *Immunity* **7,** 273–282
12. Samaridis, J., and Colonna, M. (1997) *Eur. J. Immunol.* **27,** 660–665
13. Saverino, D., Fabbi, M., Ghiotto, F., Merlo, A., Bruno, S., Zarcone, D.,

Tenca, C., Tiso, M., Santoro, G., Anastasi, G., Cosman, D., Grossi, C. E., and Ciccone, E. (2000) *J. Immunol.* **165,** 3742–3755
14. Lanier, L. L. (2005) *Annu. Rev. Immunol.* **23,** 225–274
15. Volz, A., Wende, H., Laun, K., and Ziegler, A. (2001) *Immunol. Rev.* **181,** 39–51
16. Colonna, M., Nakajima, H., and Cella, M. (2000) *Semin. Immunol.* **12,** 121–127
17. Dietrich, J., Nakajima, H., and Colonna, M. (2000) *Microbes Infect.* **2,** 323–329
18. Fanger, N. A., Cosman, D., Peterson, L., Braddy, S. C., Maliszewski, C. R., and Borges, L. (1998) *Eur. J. Immunol.* **28,** 3423–3434
19. Morel, E., and Bellón, T. (2008) *J. Immunol.* **181,** 2368–2381
20. Prod'homme, V., Griffin, C., Aicheler, R. J., Wang, E. C., McSharry, B. P., Rickards, C. R., Stanton, R. J., Borysiewicz, L. K., López-Botet, M., Wilkinson, G. W., and Tomasec, P. (2007) *J. Immunol.* **178,** 4473–4481
21. Liu, W. R., Kim, J., Nwankwo, C., Ashworth, L. K., and Arm, J. P. (2000) *Immunogenetics* **51,** 659–669
22. Young, N. T., Canavez, F., Uhrberg, M., Shum, B. P., and Parham, P. (2001) *Immunogenetics* **53,** 270–278
23. Bellón, T., Kitzig, F., Sayós, J., and López-Botet, M. (2002) *J. Immunol.* **168,** 3351–3359
24. Sayós, J., Martínez-Barriocanal, A., Kitzig, F., Bellón, T., and López-Botet, M. (2004) *Biochem. Biophys. Res. Commun.* **324,** 640–647
25. Cao, W., Rosen, D. B., Ito, T., Bover, L., Bao, M., Watanabe, G., Yao, Z., Zhang, L., Lanier, L. L., and Liu, Y. J. (2006) *J. Exp. Med.* **203,** 1399–1405
26. Nakajima, H., Samaridis, J., Angman, L., and Colonna, M. (1999) *J. Immunol.* **162,** 5–8
27. Chapman, T. L., Heikeman, A. P., and Bjorkman, P. J. (1999) *Immunity* **11,** 603–613
28. Chen, Y., Chu, F., Gao, F., Zhou, B., and Gao, G. F. (2007) *Protein Expr. Purif.* **56,** 253–260
29. Chapman, T. L., Heikema, A. P., West, A. P., Jr., and Bjorkman, P. J. (2000) *Immunity* **13,** 727–736
30. Shiroishi, M., Kuroki, K., Rasubala, L., Tsumoto, K., Kumagai, I., Kurimoto, E., Kato, K., Kohda, D., and Maenaka, K. (2006) *Proc. Natl. Acad. Sci. U.S.A.* **103,** 16412–16417
31. Shiroishi, M., Kajikawa, M., Kuroki, K., Ose, T., Kohda, D., and Maenaka, K. (2006) *J. Biol. Chem.* **281,** 19536–19544
32. Willcox, B. E., Thomas, L. M., and Bjorkman, P. J. (2003) *Nat. Immunol.* **4,** 913–919
33. Willcox, B. E., Thomas, L. M., Chapman, T. L., Heikema, A. P., West, A. P., Jr., and Bjorkman, P. J. (2002) *BMC Struct. Biol.* **2,** 6
34. Cao, W., Bover, L., Cho, M., Wen, X., Hanabuchi, S., Bao, M., Rosen, D. B., Wang, Y. H., Shaw, J. L., Du, Q., Li, C., Arai, N., Yao, Z., Lanier, L. L., and Liu, Y. J. (2009) *J. Exp. Med.* **206,** 1603–1614
35. Cella, M., Döhring, C., Samaridis, J., Dessing, M., Brockhaus, M., Lanzavecchia, A., and Colonna, M. (1997) *J. Exp. Med.* **185,** 1743–1751
36. Suciu-Foca, N., and Cortesini, R. (2007) *Cell. Immunol.* **248,** 59–67
37. Suciu-Foca, N., Manavalan, J. S., Scotto, L., Kim-Schulze, S., Galluzzo, S., Naiyer, A. J., Fan, J., Vlad, G., and Cortesini, R. (2005) *Int. Immunopharmacol.* **5,** 7–11
38. Vlad, G., Cortesini, R., and Suciu-Foca, N. (2008) *Hum. Immunol.* **69,** 681–686
39. Chang, C. C., Ciubotariu, R., Manavalan, J. S., Yuan, J., Colovai, A. I., Piazza, F., Lederman, S., Colonna, M., Cortesini, R., Dalla-Favera, R., and Suciu-Foca, N. (2002) *Nat. Immunol.* **3,** 237–243
40. Gleissner, C. A., Zastrow, A., Klingenberg, R., Kluger, M. S., Konstandin, M., Celik, S., Haemmerling, S., Shankar, V., Giese, T., Katus, H. A., and Dengler, T. J. (2007) *Eur. J. Immunol.* **37,** 177–192
41. Manavalan, J. S., Kim-Schulze, S., Scotto, L., Naiyer, A. J., Vlad, G., Colombo, P. C., Marboe, C., Mancini, D., Cortesini, R., and Suciu-Foca, N. (2004) *Int. Immunol.* **16,** 1055–1068
42. Manavalan, J. S., Rossi, P. C., Vlad, G., Piazza, F., Yarilina, A., Cortesini, R., Mancini, D., and Suciu-Foca, N. (2003) *Transpl. Immunol.* **11,** 245–258
43. Svajger, U., Vidmar, A., and Jeras, M. (2008) *Int. Immunopharmacol.* **8,** 997–1005
44. Kim-Schulze, S., Scotto, L., Vlad, G., Piazza, F., Lin, H., Liu, Z., Cortesini, R., and Suciu-Foca, N. (2006) *J. Immunol.* **176,** 2790–2798
45. Suciu-Foca, N., Feirt, N., Zhang, Q. Y., Vlad, G., Liu, Z., Lin, H., Chang, C. C., Ho, E. K., Colovai, A. I., Kaufman, H., D'Agati, V. D., Thaker, H. M., Remotti, H., Galluzzo, S., Cinti, P., Rabitti, C., Allendorf, J., Chabot, J., Caricato, M., Coppola, R., Berloco, P., and Cortesini, R. (2007) *J. Immunol.* **178,** 7432–7441
46. Borges, L., Kubin, M., and Kuhlman, T. (2003) *Blood* **101,** 1484–1486
47. Garner, L. I., Salim, M., Mohammed, F., and Willcox, B. E. (2006) *Protein. Expr. Purif.* **47,** 490–497
48. Gao, G. F., Tormo, J., Gerth, U. C., Wyer, J. R., McMichael, A. J., Stuart, D. I., Bell, J. I., Jones, E. Y., and Jakobsen, B. K. (1997) *Nature* **387,** 630–634
49. Willcox, B. E., Gao, G. F., Wyer, J. R., O'Callaghan, C. A., Boulter, J. M., Jones, E. Y., van der Merwe, P. A., Bell, J. I., and Jakobsen, B. K. (1999) *Protein Sci.* **8,** 2418–2423
50. Schuck, P. (2000) *Biophys. J.* **78,** 1606–1619
51. Otwinowski, Z., and Minor, W. (1997) *Methods Enzymol.* **276,** 307–326
52. Matthews, B.W. (1968) *J. Mol. Biol.* **33,** 491–497
53. Vagin, A., and Teplyakov, A. (1997) *J. Appl. Crystallogr.* **30,** 1022–1025
54. McCoy, A. J., Grosse-Kunstleve, R. W., Adams, P. D., Winn, M. D., Storoni, L. C., Read, R. J., (2007) *J. Appl. Crystallogr.* **40,** 658–674
55. CCP4 (1994) *Acta Crystallogr. D Biol. Crystallogr.* **50,** 760–763
56. Murshudov, G. N., Vagin, A. A., and Dodson, E. J. (1997) *Acta Crystallogr. D Biol. Crystallogr.* **53,** 240–255
57. Emsley, P., and Cowtan, K. (2004) *Acta Crystallogr. D Biol. Crystallogr.* **60,** 2126–2132
58. Vaguine, A. A., Richelle, J., and Wodak, S. J. (1999) *Acta Crystallogr. D Biol. Crystallogr.* **55,** 191–205
59. Fenn, T. D., Ringe, D., and Petsko, G. A. (2003) *J. Appl. Crystallogr.* **36,** 944–947
60. Nicholls, A., Sharp, K. A., and Honig, B. (1991) *Proteins* **11,** 281–296
61. Chen, Y., Gao, F., Chu, F., Peng, H., Zong, L., Liu, Y., Tien, P., and Gao, G. F. (2009) *J. Mol. Biol.* **386,** 841–853
62. Chen, Y., Liu, P., Gao, F., Cheng, H., Qi, J., and Gao, G. F. (2010) *Protein Cell* **1,** 153–160
63. Saulquin, X., Gastinel, L. N., and Vivier, E. (2003) *J. Exp. Med.* **197,** 933–938
64. Foster, C. E., Colonna, M., and Sun, P. D. (2003) *J. Biol. Chem.* **278,** 46081–46086
65. Snyder, G. A., Brooks, A. G., and Sun, P. D. (1999) *Proc. Natl. Acad. Sci. U.S.A.* **96,** 3864–3869
66. Porollo, A., and Meller, J. (2007) *Proteins* **66,** 630–645